Microgravity Ignition Delay of Fluorinated Ethylene Propylene Wire Insulation in Forced Flow Field

Wang K.[1], Fang J.[1]*, Wang J.W.[1], Zheng S.M.[1], Guan J.F.[2], Shah H.R.[1], Wang J.J.[1], Zhang Y.M.[1]

[1] *University of Science and Technology of China, State Key Laboratory of Fire Science, Hefei, Anhui, China*

[2] *Tsinghua University, Hefei Institute for Public Safety Research, Hefei, Anhui, China*

**Corresponding author's email: fangjun@ustc.edu.cn*

ABSTRACT

Ignition of current-taking Fluorinated ethylene propylene (FEP) insulated wire was investigated in a forced flow field in micro and normal gravities. A bursting jet was firstly observed after FEP insulation pyrolysis, and the induction time was observed before ignition occurred. Experimental and theoretical analysis show that: firstly, FEP insulation melts and decomposes, but with little liquid flow and low air permeability. The accumulated volatile gas inflates, causing jet bursting in both normal gravity and microgravity. Secondly, the forced flow and gravity has little effect on the core heating time and the bursting time, while the pyrolysis time increases slightly with increasing air velocity. Thirdly, the stretch rates in terms of the velocity gradients are higher in microgravity. In this work, the stretch rates are all positive indicating positively stretched flames. Both forced flow and gravity have significant effects on the induction time, which is dependent on the stretch rate and Damkohler numbers. Induction time increases with increasing air velocity, and is higher in microgravity. Finally, the ignition delay time is dominated by the core heating and bursting time, while its bigger value and faster increase in microgravity with increasing air velocity is dominated by the induction time.

KEYWORDS: Microgravity, ignition, FEP, wire insulation, bursting jet, stretch.

NOMENCLATURE

A	Area
A_{pre}	Pre-exponential factor
Bi	Biot number
c	Specific heat capacity
d_s	Thickness of the insulation
D	Diameter of the wire
D_g	Molecular diffusion coefficient
E	Activation energy
g	Gravity acceleration
g'	Buoyancy acceleration
$\tilde{h}$	Convection heat transfer coefficient
k	Thermal conductivity
K	Stretch rate in the axial direction
t_{in}	Time of induction
t_{mix}	Time of gas mixing
t_p	Time of insulation pyrolysis
T_c	Temperature of inner core
T_{cs}	Temperature of interface
T_s	Temperature of insulation
T_p	Pyrolysis temperature
u	Velocity
V_c	Core volume
Y_g	Mass fraction
z	Axial coordinate in cylindrical coordinates

Proceedings of the Ninth International Seminar on Fire and Explosion Hazards (ISFEH9), pp. 225-235
Edited by Snegirev A., Liu N.A., Tamanini F., Bradley D., Molkov V., and Chaumeix N.
Published by St. Petersburg Polytechnic University Press
ISBN: 978-5-7422-6496-5 DOI: 10.18720/spbpu/2/k19-94

l Length of the wire
$\dot{m}$ Pyrolysis rate
M_g Molar molecular weight of C_2F_4
Nu Nusselt number
p_{in} Inner pressure
p_∞ Inner pressure
Pr Prandtl number
$\dot{q}''_{conv}$ Forced convection heat loss rate per unit area
$\dot{q}''_{rad}$ Surface radiation heat loss rate per unit area
$\dot{Q}_{conv}$ Forced convection heat loss rate
$\dot{Q}_{cs}$ Conduction heat
$\dot{Q}_J$ Joule heat
$\dot{Q}_{rad}$ Surface radiation heat loss rate
r Radial coordinate in cylindrical coordinates
r_c Radius of the core
R Ideal gas constant
Re Reynolds number
t_{burst} Time of insulation bursting
t_c Time of core heating
t_{ig} Time of ignition delay

Greek

α_{Vs} Volume augmentation coefficient of the insulation
β parameter
Γ Parameter
δ Surface tension
ΔH_R Combustion heat of C_2F_4
ΔT Temperature difference
ε Emissivity
θ Angular coordinate in cylindrical coordinates
Λ_0 Damkohler number
ν Viscosity coefficient
ρ Density
ρ_R Electrical conductivity
σ Stefan-Boltzmann constant

Subscripts

0 ambient
c Core
s Insulation
j Jet flow
g Gas
$\infty,0$ Ambient and initial condition

INTRODUCTION

A number of theoretical and experimental studies have been conducted on the ignition characteristics of solid materials in microgravity [1]. Previous research into solid material ignition in microgravity focused on the piloted ignition of PMMA and thin cellulosic sheets heated by external heat flux [2–5].

In spacecraft, one potential cause of fires is the combustion of insulation, beginning with short circuiting or overloading of the enclosed wires. The insulation of a thin wire has a large curvature that, when overloaded, there is spontaneous ignition, it is different from the piloted ignition of these materials in planar geometries. In 2012, an ignition-to-spread model of electrical wires was developed to systematically explain ground pilot ignition and the following transition to spread by Huang *et al*. [6]. Pioneering and extensive research into the spontaneous ignition of wire insulation in microgravity was conducted by Fujita *et al*, using mostly polyethylene (PE)-coated wires, to understand various aspects of the ignition mechanism, including the ignition limit, the minimum ignition energy, and the contributions of the oxygen concentration and the air pressure [7–10]. The microgravity flame spread limits of ETFE insulated copper wires under exposure to an external radiant flux were investigated by Fujita *et al*. [11], but the spontaneous ignition mechanism of high temperature wire insulation in microgravity is still unknown. Also, the effects of low air velocities on the spontaneous ignition of wire insulation in microgravity were barely considered.

In this work, experiments on the microgravity ignition of overloaded FEP wire insulation in a vertical forced flow with various air velocities were conducted in a 3.5-s drop tower. Theoretical predictions and experimental results for the spontaneous ignition delay time of FEP insulation in a stretched flow field in both normal gravity (1g) and microgravity (μg) conditions were then discussed.

EXPERIMENTS

Experimental setup

The experimental setup is as shown in Fig. 1. The experiments were conducted at the National Microgravity Laboratory in Beijing, China, which has a microgravity level of 10^{-5} g for approximately 3.5 s. The setup is composed of a combustion chamber with the sample wire located inside it, an airflow supply and exhaust system, a constant current supply system, and two imaging systems. The combustion chamber has internal dimensions of 15×15×25 cm.

The air supply and exhaust system produces a vertical forced airflow, with velocities ranging from 0.1 to 0.5 m/s. The imaging systems include a high-speed camera (1000 fps), combined with simultaneous low-speed imaging from the digital video (DV) cameras located (100 fps) on both sides. Details of the experimental setup can be found in Ref [12]. In the tests, the air supply and exhaust system and the imaging system worked for approximately 30 s and 5 s, respectively, before the fall of the cabin. The chamber pressure is 1 atm (100.3 kPa), and the temperature is maintained at about 300 K.

The sample under test is a nickel-chrome core wire coated with FEP (fluorinated ethylene propylene, UL1886 Approval AWG 20) insulation, with a configuration as shown in Fig. 1(c). The insulation depth, inner core diameter, and effective length of the sample are 0.075, 1, and 50 mm, respectively. Property of the wire is listed in Table 1. The electric resistance of the wire is approximately 0.1 Ω at room temperature. Both ends of the wire are connected to a constant current power supply through the electrodes of the sample holder. In the experiments, the current is set at a fixed value of 60 A, which provides Joule heat generation of approximately 0.367 kW.

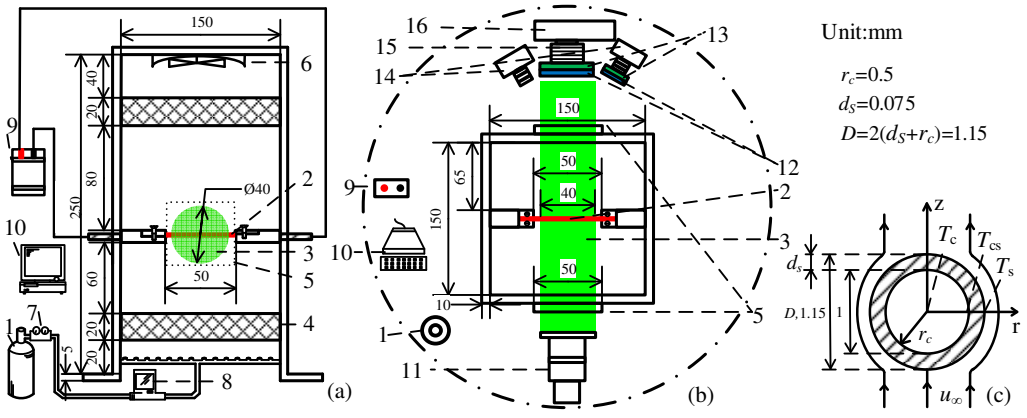

Fig. 1. Diagram of the experimental setup (a: front view; b: top view; c: wire). 1. Air supply; 2. Wire; 3. Laser beam; 4. Honeycomb; 5. Optical glass window; 6. Exhaust fan; 7. Pressure-reducing valve; 8. Flowmeter; 9. Constant current supply; 10. Computer; 11. Laser tube; 12. Neutral density (ND) filter; 13. Narrow channel filter; 14. Digital video (DV) camera; 15. Macro lens; 16. High-speed camera.

Table 1. Properties of the NiCr core and FEP insulation of the wire[a]

Wire	k, W/(m·K)	c, J/(kg·K)	ρ, kg/m^3	ρ_R, Ω·m	T_p, K	ε	δ, mN/m	l, mm
Core	12.5	450	8200	1.6×10^{-6}				50
Insulation	0.2	1170	2150		673	0.9	22.7	50

The pyrolysis of the solid FEP can be described using a zeroth-order Arrhenius law. The degraded monomer products of C_2F_4 are at a level of approximately 97%, the pre-exponential factor is 1E19 s^{-1}, and the activation energy E is 288.12 kJ/mol [13].

Chowdhury et al. proposed that the initial oxidation of C_2F_4 combustion is initiated by the attack of molecular oxygen on C_2F_4, where COF_2 is mainly formed via a dioxetane intermediate [14]:

$$F_2C{=}CF_2 + O_2 \rightarrow F_2C(O{-}O)CF_2 \rightarrow 2COF_2 \quad . \tag{1}$$

Here, the pre-exponential factor A_{pre} is 1e13 g/(m^3·s), the dimensionless activation parameter E/RT at room temperature (300 K) is 20.45, and the heat of combustion is 10.6 kJ/g [14].

Experimental phenomenon

The extinction images in still air in μg are shown in Fig. 2, where a, b are the original sequential images, c is the division image of b/a, d is the image by removing the background of image c to highlight the invisible jet. The extinction and scattering images at visible jet bursting and ignition time in μg and 1g are shown in Fig. 3, where the green images show the extinction and scattering images of the fine particles of the volatile 'condensed fraction' [13]. It is observed that the insulation initially inflates, and then bursts in the middle, where the opening size is of the same order of magnitude as the wire diameter, and then ignites within a short delay time under continuous heating. Before bursting, the inflation processes in 1g and μg are similar, but after bursting, the jet and the flame in μg are wider and the delay time is longer. Jet bursting and delayed ignition were found in all other experiments with airflows.

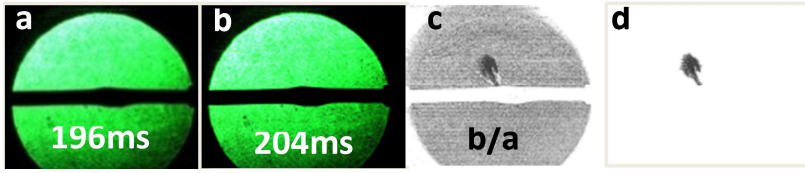

Fig. 2. Original extinction images (a, b) and division images (c, d) in still air in μg.

For the PE insulation, ignition occurs around the molten volume without jet bursting, and forms a spherical flame in μg [10]. The FEP insulation melts and decomposes, but the molten FEP demonstrates great tenacity with little liquid flow and low air permeability [13]. Because the insulation was sealed in the two hold positions, the accumulated volatile gas is increasingly inflated with increasing time, which aggravates the reduced heating of the outer surface. In the center of the wire, the expansion stress is higher, and bursting thus occurs more easily here, where a jet flame is formed in both 1g and μg. The bursting direction is random, but is mostly vertical under the induction of a vertical airflow for reduced convection heat loss on the upper surface. In this work, all analyses were based on the results for vertical bursting jets in the central position.

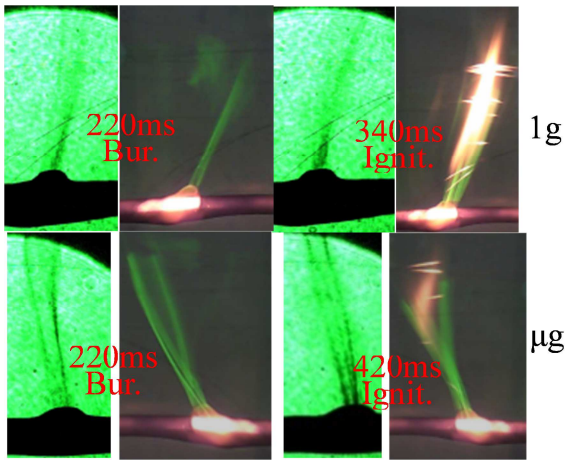

Fig. 3. Extinction and scattering images at bursting (Bur.) and ignition (Ignit.) time in still air in 1g and μg.

As shown in Fig. 3, the critical bursting time was determined when the total number of pixels of the jet flow in the extinction images (1280×1024 pixels) first exceeded the threshold of 20,800, which corresponds to the obvious visible jet shown in the scattering images. The ignition time was determined when total pixels of the flashing flame in the scattering images (720×1280 pixels) first exceed the threshold of 3,000. The jet flow velocity was calculated by the jet front moving distance divided by the travel time using the processed jet images as shown in Fig. 2(d). Data of 1g condition are given as the average of three repeated tests, while data of the μg condition are from a single test under each condition for the limitations of the microgravity test numbers. The error for both the bursting time and the ignition time is approximately 3 ms.

THEORETICAL METHODS

The experiments show that, after jet bursting and mixing, no intense gas-phase reaction appears to follow rapidly in the flow field of the vaporized fuel gas and the hot oxidant gas. In forced flow with a stretched flow field, a high stretch rate for the velocity gradient will result in longer ignition delays, where a chemical induction time may be needed before ignition [15]. The chemical reaction time for gas combustion is often less than 1 ms, and was thus ignored. The ignition delay time t_{ig} thus includes the core heating, insulation pyrolysis, insulation bursting, gas mixing and gas induction times: $t_{ig} = t_c + t_p + t_b + t_{mix} + t_{in}$. Here we define $t_c + t_p + t_b$ is the total pyrolysis time, $t_{mix} + t_{in}$ is the total induction time. In the experiments, either the total pyrolysis time or total induction time is very difficult to be determined from the video. We define that when there is critical bursting, the time is $t_c + t_p + t_b$, after that, it is the total induction time of $t_{mix} + t_{in}$.

Total pyrolysis time

Core heating time

The energy balance of the wire core is given by:

$$\rho_c c_c V_c \left(dT_c/dt\right) = \dot{Q}_J - \dot{Q}_{cs}, \tag{2}$$

where $\dot{Q}_J$ is the Joule heat that is generated in the core of RI^2, V_c is the core volume, and $\dot{Q}_{cs}$ is the conduction heat given by the wire core to heat the insulation to the pyrolysis temperature of T_p, which is described as:

$$\dot{Q}_{cs} = k_s \frac{T_{cs} - T_p}{r_c \ln\left(\left(d_s + r_c\right)/r_c\right)} A_c = 2\pi k_s l \frac{T_{cs} - T_p}{\ln\left(\left(d_s + r_c\right)/r_c\right)}, \tag{3}$$

where $T_{cs} = T_c - \dot{Q}_J / 2\pi k_c l$, which was independently measured based on the penetration of a thermocouple under steady-state conditions and without imaging measurements. In the experiments, T_{cs} is approximately 1300 K. Here we define $a_1 = \rho_c c_c V_c$, $b_1 = -2\pi k_s l / \ln\left(\left(d_s + r_c\right)/r_c\right)$ and $c_1 = \left(1 + \frac{k_s}{k_c \ln\left(\left(d_s + r_c\right)/r_c\right)}\right)\dot{Q}_J + \frac{2\pi k_s l}{\ln\left(\left(d_s + r_c\right)/r_c\right)} T_p$. Then, the time taken for the inner core to be heated to a temperature T_c can be integrated from Eq. (2) as:

$$t_c = \left(a_1/b_1\right) \ln\left(\left(b_1 T_c + c_1\right)/\left(b_1 T_0 + c_1\right)\right). \tag{4}$$

Pyrolysis time

The pyrolysis time is defined as the time taken for the insulation to be heated to the pyrolysis temperature T_p, without consideration of the complex inflation process. The insulation material is thermally thin as the Biot number $Bi = h d_s / k_s$ is between 0.0036 and 0.0271, which is smaller than the threshold of 0.1 [16]. The insulation heat losses are dominated by forced convection $\dot{Q}_{conv}$ and surface radiation $\dot{Q}_{rad}$, such that the energy balance of the insulation is:

$$\rho_s c_s V_s \left(dT_s/dt\right) = \dot{Q}_{cs} - \dot{Q}_{conv} - \dot{Q}_{rad}, \tag{5}$$

where V_s is the volume of the insulation, $\dot{Q}_{conv} = \dot{q}''_{conv} A_s = 2\pi\left(d_s + r_c\right) l \tilde{h} \left(T_s - T_\infty\right)$, and $\dot{Q}_{rad} = \dot{q}''_{rad} A_s = 2\pi\left(d_s + r_c\right) l \varepsilon\sigma \left(T_s^4 - T_\infty^4\right)$. Here we assume that $T_s^4 - T_\infty^4 \approx 4T_\infty^3 \left(T_s - T_\infty\right)$, and define $a_2 = \rho_s c_s V_s$ and $b_2 = \dot{Q}_{cs}$. Then the pyrolysis time t_p can be integrated via Eq. (5) by combining Eq. (3) with two heat loss equations:

$$t_p = -\left(a_2/c_2\right) \ln\left(1 - c_2/b_2 \left(T_p - T_\infty\right)\right). \tag{6}$$

Bursting time

The pressure jump across the interface of the insulation is balanced by the curvature force at the interface, which is described as : $p_{in} - p_\infty = \delta \nabla \mathbf{n}$, where the inner pressure p_{in} is caused by the hot volatile gas generated by pyrolysis. In a cylinder, the curvature of a circular surface is: $\nabla \mathbf{n} = \nabla \bar{r} = \left(\partial r^2/\partial r\right)/r^2 = 2/r$. To simplify this problem, we assume here that: all pyrolysis gases were accumulated below a very thin outer surface; the pyrolysis gas inside maintained the constant temperature of T_p; and the ideal law applies to the pyrolysis gases. Thus, at the bursting time t_b, $p_{in} V_{g(in)} = \left(\dot{m} t_b / M_g\right) R T_p$, where $\dot{m}$ is the pyrolysis rate (g/s), M_g is the molar molecular weight of C_2F_4, and R is the ideal gas constant (8.31 J/K.mol).

Therefore, at the critical bursting condition, $\dot{m}t_b/M_g V_{g(in)} RT_p = p_\infty + 2\delta/(d_s + r_c)$, where the inflated gas volume is $V_{g(in)} = \pi\left((d_s + r_c)^2 - r_c^2\right)l = \alpha_{Vs} V_s$, and α_{Vs} is the volume augmentation coefficient of the insulation, which can be determined via image analysis. The insulation pyrolysis is described using a zeroth-order Arrhenius law, where the pyrolysis rate is $\dot{m} = A_{pre}\rho_s \exp(-E/RT_p)V_s$. Therefore, the bursting time is

$$t_b = \alpha_{Vs} \frac{M_g}{A_{pre}\rho_s RT_p}\left(p_\infty + \frac{2}{d_s + r_c}\delta\right)\exp\left(\frac{E}{RT_p}\right). \tag{7}$$

Total induction time

Mixing time

The bursting gas is mixed with air by molecular or convection diffusion, and if axial diffusion is neglected, then the mixing time can be described as the following radial diffusion time:

$$t_{mix} = (D/2)^2 / D_g \ , \tag{8}$$

where D_g is the molecular diffusion coefficient of C_2F_4 at $T_g = (T_p + T_\infty)/2$.

Induction time

In 1981, Niioka [17] provided an induction time formula for a counterflow flame, but no such analysis has been performed for the co-flow problem. Because the stretch rate of the counterflow is $2K$ in the axial direction, while the rate is K for co-flow, we rewrite the formulas here to provide order-of-magnitude estimates:

$$t_{in} = -\ln(1 - \Gamma/\Lambda_0)/2K \ , \tag{9}$$

where K is the stretch rate in the axial direction, Λ_0 is the Damkohler number, which is given by $\Lambda_0 = \frac{1}{K}\frac{A_g \Delta H_R}{\rho_g c_p T_\infty}\left(\frac{E}{RT_\infty}\right)\exp\left(-\frac{E}{RT_\infty}\right)$, $\Gamma = 4(E/RT_\infty)\left((2-\beta)/e^2(1-\beta^2)\right)$, and $\beta = T_\infty c_p / Y_g \Delta H_R$ [14], where ΔH_R is the combustion heat of C_2F_4, Y_g is the mass fraction, and c_p is the specific heat at a constant pressure.

The stretch rate is defined as [18]:

$$K = -\mathbf{n}\cdot\nabla\times(\mathbf{v}_s \times \mathbf{n}) + (\mathbf{V}_f \cdot \mathbf{n})(\nabla \cdot \mathbf{n}) \ . \tag{10}$$

For a cylindrical model of the jet flow, while assuming that the axial velocity is uniform across the sectional area, adopting cylindrical (r, θ, z) coordinates, and using Eq. (10), in which $\mathbf{V}_f = 0$, $\mathbf{v} = (0, 0, -u)$, and $\mathbf{n} = (-1, 0, 0)$, we then have $K = -du/dz$, where $u = u_j + u_\infty$ is the local jet flow velocity in a co-flow environment, which can be covered using a decay and an average second buoyancy acceleration [19].

$$u = 0.375\,\mathrm{Re}_j\,(D/2)u_0/z + 0.5\sqrt{2g'z} \ , \tag{11}$$

where $\mathrm{Re}_j = u_{j0}D/2\nu_g$, $u_0 = u_{j0} + u_\infty$, and $z \in [D/2,\ l_j]$, the buoyancy acceleration is $g' = g(\rho_\infty - \rho_j)/\rho_j = g(T_p - T_\infty)/T_\infty$, and in microgravity, $g' = 0$.

The stretch rate then becomes:

$$K = 0.375\,\mathrm{Re}_j\,(D/2)u_0/z^2 - 0.25\sqrt{2g'}/z^{1/2}\ . \tag{12}$$

Then at a length l_j, the stretch rate is $K = 0.375\,\mathrm{Re}_j\,(D/2)(u_{j0}+u_\infty)l_j^{-2} - 0.25\sqrt{2g'}\,l_j^{-0.5}$. In normal gravity, if l_j is smaller than the critical value of $l_{j(cri)}|_{K=0} = \left(0.75\,\mathrm{Re}_j\,D(u_{j0}+u_\infty)/\sqrt{2g'}\right)^{1/1.5}$, $K > 0$. In microgravity, $K = 0.375\,\mathrm{Re}_j\,(D/2)(u_{j0}+u_\infty)l_j^{-2} > 0$, which indicates that the flame is positively stretched.

ANALYSIS AND DISCUSSION

Total pyrolysis time

The experimental and theoretical predictions of t_c, t_p and t_b are shown in Fig. 4. Bursting is seen to be dominant in the time regime, and forced flow and gravity have no effects on t_c and t_b. The pyrolysis time t_p is very short, but it increases with increasing air velocity.

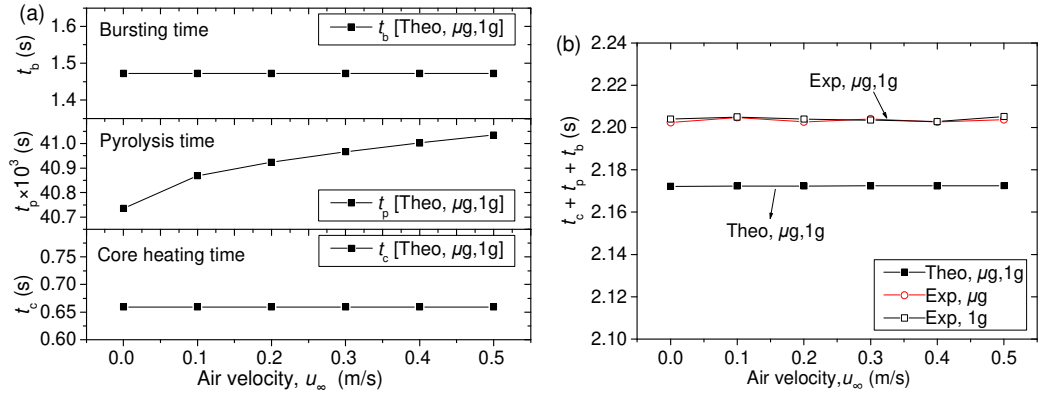

(a) (b)

Fig. 4. (a) Theoretical core heating time, pyrolysis time and bursting time; (b) theoretical and experimental total times.

Total induction time

The values of t_{mix} under 1g and μg conditions are approximately the same at about 0.01 s, based on Eq. (8). The experimental jet lengths under 1g and μg conditions and the theoretical critical jet length are as shown in Fig. 5. The jet length is defined as the jet moving distance between the bottom and tip at the critical bursting time, which was obtained by the image analysis. With increasing air velocity, l_j also increases. Under 1g conditions, l_j is larger than that under μg conditions, but is smaller than the critical jet length of $l_{j(cri)}|_{K=0} = \left(0.75\,\mathrm{Re}_j\,D(u_{j0}+u_\infty)/\sqrt{2g'}\right)^{1/1.5}$; thus, based on Eq. (12), $K > 0$, which means that the flames are positively stretched under both 1g and μg conditions.

The theoretical Damkohler numbers and stretch rates under 1g and μg conditions at the jet lengths are as shown in Fig. 6. The stretch rate increases with increasing air velocity, while in μg, the rate is higher, as indicated by Eq. (12). Correspondingly, the Damkohler number is higher under 1g conditions and decreases more rapidly.

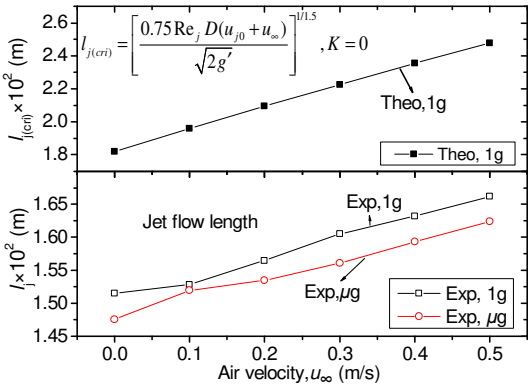

Fig. 5. Experimental jet lengths under 1g and μg conditions, and theoretical critical jet lengths in 1g.

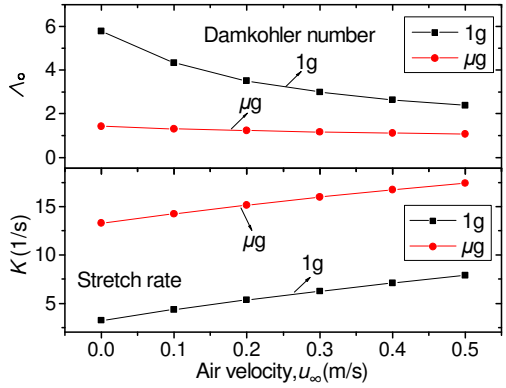

Fig. 6. Theoretical Damkohler numbers and stretch rates at jet lengths.

The theoretical induction times with the stretch rates under 1g and μg conditions are as shown in Fig. 7. With increasing stretch rate, the induction time also increases. The experimental and theoretical total times of mixing and induction times and their ratios in 1g and μg are as shown in Fig. 8. It can also be seen that in μg, t_{in} increases more rapidly with increasing air velocity, and is approximately twice the corresponding value in 1g.

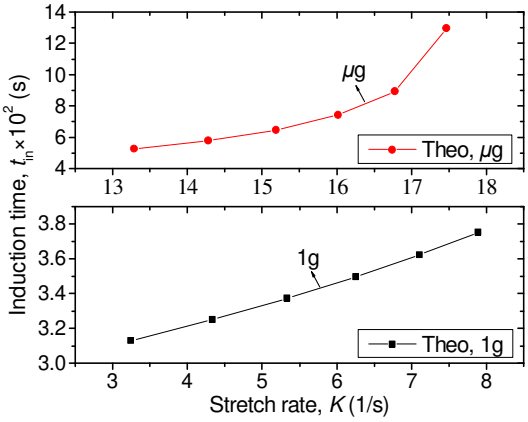

Fig. 7. Theoretical induction time with stretch rate.

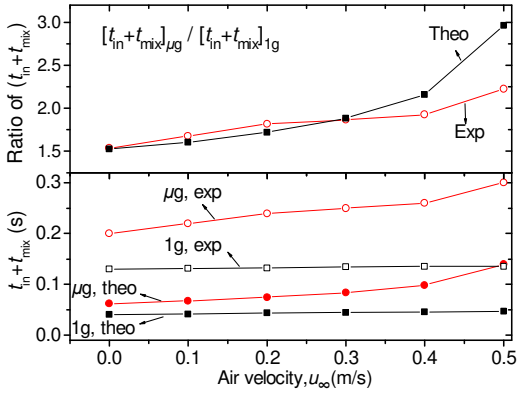

Fig. 8. Experimental and theoretical induction and mixing times and ratios with air velocity (t_{mix}=0.01s).

Ignition delay time

The experimental and theoretical total times for the ignition delay are as shown in Fig. 9. t_c and t_b dominate the delay time, with little effect from both forced flow and gravity. As t_p and t_{mix} are small, t_{in} increases significantly and is higher in μg, therefore, the higher and faster increase of ignition delay time in μg is dominated by the induction time t_{in}.

CONCLUSIONS

The stretch rates in terms of their velocity gradients are higher in microgravity without the contributions of buoyancy, and increase with increasing air velocities. In this work, all stretch rates are positive, thus indicating positively stretched flames, while the Damkohler numbers are higher in microgravity, thus indicating longer residence times, and they decrease with increasing air velocity.

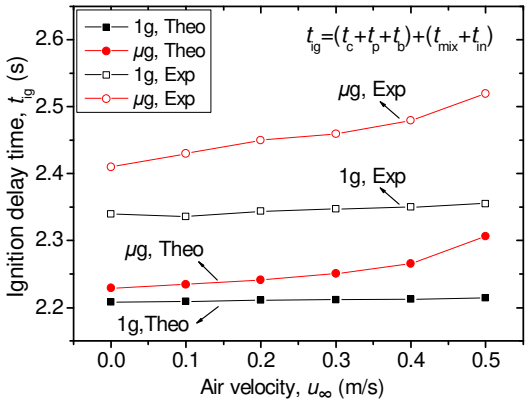

Fig. 9. Experimental and theoretical ignition delay times with air velocity.

Forced flow and gravity have significant effects on the induction time, which is dependent upon the stretch rate and Da number. The induction time increases with increasing air velocity, and in microgravity it is higher.

The ignition delay time is dominated by the core heating and bursting time, while its bigger value and faster increase in microgravity with increasing air velocity is dominated by the induction time.

ACKNOWLEDGEMENT

This work was sponsored by the National Natural Science Foundation of China (No. 51636008, 51576186, 51323010), Key Research Program of the Chinese Academy of Sciences (NO. QYZDB-SSW-JSC029), National Key R&D Program (2016YFC0801504) and Fundamental Research Funds for the Central Universities (WK2320000036). Fang Jun expresses sincere appreciation to Prof. Forman A. Williams for his valuable suggestions during the visit to UCSD.

REFERENCES

[1] Fujita O, Solid combustion research in microgravity as a basis of fire safety in space, Proc. Combust. Inst. 35 (2015) 2487-2502.

[2] Y. Nakamura, H. Yamashita, T. Takeno, et al, Effects of gravity and ambient oxygen on a gas-phase ignition over a heated solid fuel, Combust. Flame 120 (2000) 34-48.

[3] S.L. Olson, T. Kashiwagi, O. Fujita et al, Experimental observations of spot radiative ignition and subsequent three-dimensional flame spread over thin cellulose fuels, Combust. Flame 125 (2001) 852-864.

[4] S. McAllister, C. Fernandez-Pello, D. Urban et al, The combined effect of pressure and oxygen concentration on piloted ignition of a solid combustible, Combust. Flame 157 (2010) 1753-1759.

[5] S.L. Olson, Piloted ignition delay times of opposed and concurrent flame spread over a thermally-thin fuel in a forced convective microgravity environment, Proc. Combust. Inst. 33 (2011) 2633-2639.

[6] X. Huang, Y. Nakamura, F.A. Williams, Ignition-to-spread transition of externally heated electrical wire, Proc. Combust. Inst. 34 (2013) 2505-2512.

[7] Y. Nakamura, N. Yoshimura, H. Ito et al, Flame spread over electric wire in sub-atmospheric pressure, Proc. Combust. Inst. 32 (2009) 2559-2566.

[8] O. Fujita, T. Kyono, Y. Kido et al, Ignition of electrical wire insulation with short-term excess electric current in microgravity, Proc. Combust. Inst. 33 (2011) 2617-2623.

[9] Y. Takano, O. Fujita, N. Shigeta et al, Ignition limits of short-term overloaded electric wires in microgravity, Proc. Combust. Inst. 34 (2013) 2665-2673.

[10] S. Takahashi, H. Takeuchi, H. Ito et al, Study on unsteady molten insulation volume change during flame spreading over wire insulation in microgravity, Proc. Combust. Inst. 34 (2013) 2657-2664.

[11] A.F. Osorio, K. Mizutani, C. Fernandez-Pello et al, Microgravity flammability limits of ETFE insulated wires exposed to external radiation, Proc. Combust. Inst. 35 (2015) 2683-2689.

[12 J.F. Guan, J. Fang, Y. Xue et al, Morphology and concentration of smoke from fluorinated ethylene propylene wire insulation in microgravity under forced airflow, J. Hazard. Mater. 320 (2016) 602-611.

[13] S. Straus, L.A. Wall, Pyrolysis of Polyarnides, J. Res. Natl. Bur. Stand. 60 (1958) 39-45.

[14] C.H. Douglass, H.D. Ladouceur, V.A. Shamamian et al, Combustion chemistry in premixed C_2F_4-O_2 flames, Combust. Flame 100 (1995) 529-542.

[15] G. Cox, Combustion Fundamentals of Fire, Academic Press, London, 1995, pp. 44.

[16] S. McAllisterl, J.Y. Chen, A.C. Fernandez-Pello, Fundamentals of Combustion Processes, Springer Press, New York,2011, pp.104.

[17] T. Niioka, Ignition time in the stretched-flow field, Proc. Combust. Inst. 18 (1981) 1807-1813.

[18] C.K. Law, Combustion Physics, Cambridge University Press, New York, 2006, 407 p.

[19] S.R. Turns, An Introduction to Combustion, 2nd Ed., McGraw-Hill, Boston, Massachusetts, 2000, 310 p.